High-Resolution Interaction with Corotational Coarsening Models

Rosell Torres[1]   Alejandro Rodríguez[2]   José M. Espadero[1]   Miguel A. Otaduy[1]

[1]URJC Madrid   [2]University of Granada

Figure 1: *Interactive deformation of a CT data set discretized with $281K$ tetrahedra. With our corotational coarsening method, we represent this complex model using a coarse mesh with $6K$ tetrahedra, which captures the high-resolution heterogeneity of the original model. As shown in the examples, we can impose accurate boundary conditions at arbitrary locations within the volume (see the yellow ball pulling from the veins, or the cylindrical tool in contact with the kidney).*

Abstract

This paper presents a numerical coarsening method for corotational elasticity, which enables interactive large deformation of high-resolution heterogeneous objects. Our method derives a coarse elastic model from a high-resolution discretization of corotational elasticity with high-resolution boundary conditions. This is in contrast to previous coarsening methods, which derive a coarse elastic model from an unconstrained high-resolution discretization of regular linear elasticity, and then apply corotational computations directly on the coarse setting. We show that previous approaches fail to handle high-resolution boundary conditions correctly, suffering accuracy and robustness problems. Our method, on the other hand, supports efficiently accurate high-resolution boundary conditions, which are fundamental for rich interaction with high-resolution heterogeneous models. We demonstrate the potential of our method for interactive deformation of complex medical imaging data sets.

Keywords: Elasticity, homogenization, coarsening

Concepts: •**Computing methodologies → Physical simulation;**

1 Introduction

Real-world objects are often heterogeneous. This heterogeneity competes with interactive simulation requirements, because heterogeneity produces deformations that are highly nonlinear w.r.t. material coordinates, and this in turn requires high-resolution discretizations. Living tissue is the archetypal example of heterogeneous material, and planning of surgical interventions is a highly relevant application that is hampered by the difficulty of resolving the deformation of heterogeneous tissues in an interactive manner.

Coarsening or homogenization methods have been introduced as an approach to accurately approximate high-resolution heterogeneous materials using low-resolution discretizations. They do this by estimating as a preprocess a locally homogeneous material that best approximates heterogeneous behavior. Kharevych et al. [2009] and Nesme et al. [2009] presented concurrently two different methods for coarsening of heterogeneous elastic objects in computer graphics. Later, Torres et al. [2014] extended the method of Nesme et al. with a more flexible coarsening strategy. All these methods derive homogenization techniques for linear elasticity and apply a corotational formulation in the coarse setting. The first important result in our paper is a demonstration that, *only for unconstrained problems*, applying a corotational formulation on a coarsened linear problem is equivalent to coarsening a high-resolution corotational formulation with uniform rotation. As a corollary, we also demonstrate that this equivalence is not true for problems with high-resolution boundary conditions, and we show that naïve solutions suffer notable accuracy and robustness problems. The derivation of our basic coarsening method for unconstrained corotational problems, described in Section 3, sets the basis for coarsening more complex constrained problems later.

In Section 4, we derive a coarsening method for linear corotational elasticity problems with high-resolution boundary conditions. While the method is computationally costly for general boundary conditions, we show how to derive accurate yet efficient coarsened representations for certain interesting types of boundary conditions, with a computational cost on par with that of a regular coarse simulation. In particular, we develop efficient solutions for static Dirichlet conditions and low-rank Neumann conditions. Handling these types of boundary conditions appears computationally expensive at first sight too, but we show how to handle them efficiently thanks to carefully selected linear algebra operations.

With interactive surgical planning as one of the target applications of heterogeneous materials, we pay special attention to the design of efficient deformation models on volumetric data sets. In Section 5, we describe a method to efficiently transfer the coarse corotational deformation to a volumetric data set, following a massively parallel rasterization approach.

Fig. 1 demonstrates the ability of our method to perform interactive yet accurate fine deformations on a complex volumetric data set with 281K tetrahedra. A regular FEM deformation runs at 0.4 fps on this mesh. Thanks to our coarsening method, we achieve a similar accuracy using a mesh of 6K tetrahedra, at interactive deformation rates of 30 fps. We increase accuracy by one order of magnitude w.r.t. a regular coarse simulation of the same resolution, under practically the same cost. The full simulation and visualization, including contact, deformation, rasterization, and high-resolution volume rendering of the deformed data set run at 10 fps. The snapshots show how we can pull from arbitrary locations within the volume (see the yellow ball pulling from the veins), or apply high-resolution contacts (see the cylindrical tool interacting with the kidney), and the deformations robustly and accurately capture the high-resolution heterogeneity of the data. The accurate fine deformations shown in the examples are not possible with regular coarse simulations or previous coarsening methods. In Section 6 we discuss additional experiments and results.

2 Related Work

There are three major approaches to achieve cost-effective simulation of high-resolution deformable objects: coarsening or homogenization, subspace deformation, and adaptive discretization. Coarsening methods optimize the parameters of a coarse model as a preprocess, such that its behavior accurately approximates the behavior of the underlying heterogeneous object. The coarsening process is also called homogenization because the heterogeneous material is locally homogenized. Coarsening methods differ in terms of the coarse model of choice and the metric that is optimized.

The theory of homogenization spans several decades in the field of computational mechanics, and we refer to the survey by Cioranescu and Donato [2000] for an overview. Early homogenization approaches made restrictive assumptions on material parameters, such as periodicity [Michel et al. 1999]. Filonova et al. [2013] have recently designed a corotational homogenization method for reduced deformations, but their method also assumes material periodicity within a single corotational frame. Owhadi and Zhang [2007] introduced a more versatile homogenization approach for problems such as elastostatics for the 1D case.

This approach was extended by Kharevych et al. [2009] to design a homogenization technique for 3D elastostatic problems within computer graphics. Their technique estimates per-coarse-element linear material tensors, maximizing the similarity of potential energies under a test set of boundary displacements. They formulated homogenization as a global problem on the full object, but the approach was later extended to solve smaller problems on subdomains [Owhadi, Houman et al. 2014]. Concurrently to Kharevych et al., Nesme et al. [2009] proposed a coarsening technique that operates per coarse element and Cartesian coordinate. It estimates per-coarse-element 1D stiffness matrices and shape functions that are nonlinear w.r.t. material coordinates, such that coarse and fine displacements match when forces are applied on coarse nodes only. In addition, to preserve the topology of the underlying object, they carried out coarsening in a multi-resolution fashion. Recently, Torres et al. [2014] extended Nesme's method with a more flexible coarsening strategy that works directly with the full 3D stiffness matrices. Their method can be regarded as a per-element projection of high-resolution deformations to best-fit coarse nodal deformation bases.

The original approach by Kharevych et al. can be regarded as more accurate as it seeks global similarity of elastic behavior, while the extensions by Owhadi et al. [2014] and the approach by Nesme et al. enforce only local similarity but favor sparse computations. We exploit the versatility enabled by local similarity to incorporate accurate treatment of boundary conditions, and specifically we build on the approach by Nesme et al.

Kharevych et al., Nesme et al., and Torres et al., all extended their methods to corotational elasticity in similar ways. Their methods produce coarse models for linear high-resolution elasticity, and they apply the corotational formulation as an afterthought in the coarse setting. Instead, we derive a coarse model for corotational high-resolution elascticity. We observe that, for an unconstrained high-resolution problem, our derivation reaches the same result proposed by Torres et al. However, our derivation also handles accurately high-resolution problems with Dirichlet (i.e., position) and Neumann (i.e., force) boundary conditions. Previous methods, on the other hand, fail to support accurately and robustly high-resolution boundary conditions.

Similar to homogenization, Faure et al. [2011] coarsen a heterogeneous object using a meshless frame-based discretization. To account for heterogeneity, they design nonlinear shape functions. But they do not compute homogenized material parameters, they approximate integrals in the heterogeneous volume instead. Coarsening methods have recently gained relevance in the context of computational design algorithms for digital fabrication [Chen et al. 2015; Schumacher et al. 2015; Panetta et al. 2015].

Model reduction or subspace deformation methods project the full space of possible deformations to a compact basis of deformations that approximates well the high-resolution behavior [Pentland and Williams 1989; Barbič and James 2005]. Improvements over basic approaches have aimed at decomposing the deformation into multiple local subspace models [Barbič and Zhao 2011; Kim and James 2011], contact handling [Teng et al. 2014], or coupling subspace models to localized high-resolution models [Harmon and Zorin 2013; Teng et al. 2015]. In contrast to homogenization methods, subspace deformation models typically reach a more compact basis, but their basis functions have more global support. However, it is no surprise that subspace methods and coarsening methods based on nodal projection [Nesme et al. 2009; Torres et al. 2014] share some mathematical tools, such as shape functions for the reconstruction of high-resolution deformations, Schur complements for the computation of projections [Teng et al. 2015], or couplings with efficient treatment of corotational settings [Kim and James 2011]. These shared tools will become apparent throughout the paper.

Finally, adaptive methods place degrees of freedom where necessary to maximize accuracy while minimizing the computational cost. The two main approaches are to either refine the elements [Debunne et al. 2001; Capell et al. 2002] (known as h-refinement) or the basis functions [Grinspun et al. 2002] (known as p-refinement). Adaptive methods are complementary to coarsening techniques, as one could use a coarsening technique to compute the best-fit representation in coarse areas of the adaptive discretization. To conclude, multifarious hierarchies [Malgat et al. 2015] offer a framework to combine different deformation models to achieve desired global and local properties.

3 Corotational Coarsening

This section describes the fundamentals of our coarsening method. First, we describe the coarsening strategy, which follows the ones by Nesme et al. [2009] and Torres et al. [2014]. It takes as input high-resolution and low-resolution discretizations of the deformable volume under study, and formulates coarsening on a per-element basis on the coarse discretization. Next, we formulate the high-resolution corotational elasticity problem, which we wish to coarsen. To support accurate handling of high-resolution boundary conditions, this high-resolution problem admits diverse Dirichlet

and Neumann boundary conditions imposed on the high-resolution discretization. Finally, we derive a homogenization method for the simplest, unconstrained corotational elasticity problem. The solutions for problems with complex Dirichlet and Neumann conditions will be built incrementally on the solution to the unconstrained problem in the following section.

3.1 Coarsening Strategy

We borrow from Nesme et al. [2009] the basic strategy that supports our coarsening method. Given fine and coarse discretizations of a heterogeneous linear elastic material, with the coarse nodes a subset of the fine nodes, we replace with a coarse homogeneous element its overlapping fine heterogeneous submesh, such that deformations computed using the coarse element alone fit best the deformations of the fine submesh. This strategy enables the design of a homogenization method that works on a per-coarse-element basis. The specific approach by Nesme et al. works on a multi-resolution hierarchy, with successive coarsening, and treats the deformation problem on each Cartesian axis separately. We depart from this approach and follow instead the approach by Torres et al. [2014], which coarsens from the fine to the coarse mesh directly, and handles the deformations in the three Cartesian axes simultaneously.

In practice, making the coarse nodes a subset of the fine nodes can be achieved in multiple ways, for example applying subdivision to the coarse mesh, or simply by remeshing the union of coarse and fine nodes. If the submesh overlapping a coarse element has multiple connected components, it is possible to define one coarse element for each component and consider each component as a separate submesh, thus preserving the topology of the fine mesh in a way similar to Nesme et al.

As proposed by Nesme et al., in our coarsening method, the homogeneous linear material of each coarse element is described through a coarse stiffness matrix, and deformations of coarse nodes are interpolated to fine nodes using precomputed nonlinear shape functions. The extension of the corotational coarsening method to a complete coarse mesh is simple. Per-element stiffness matrices are assembled for the complete mesh, in a way analogous to the regular corotational formulation [Müller and Gross 2004]. To compute the deformations of fine nodes belonging to the fine submeshes of multiple coarse elements, we simply average the contributions of the various elements through inverse-distance weighting.

In our examples, we have simulated quasi-static and dynamic deformations. For dynamic deformation, an accurate solution would require coarsening of mass contributions, but we have approximated coarse masses through mass lumping.

3.2 Formulation of the High-Resolution Problem

Given the fine submesh of a coarse element, we formulate a generic linear corotational elastic FEM problem on this mesh. Our derivation of a homogenization method for corotational elasticity relies on the following key assumption: a common rotation matrix serves as a good corotational frame for the complete fine submesh associated with each coarse element. Fig. 2 shows the validity of this hypothesis on one characteristic deformation example. In practice, we use polar decomposition to estimate the best-fit rotation matrix for each coarse element.

We use the notation $[\mathbf{R}]$ to denote a block-diagonal matrix formed by replicating a rotation matrix $\mathbf{R}$. In the equations in this paper, the size of $[\mathbf{R}]$ can be inferred in each case from the terms it multiplies. Following this notation, the linear corotational elasticity problem
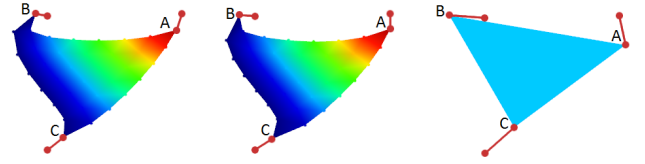
Figure 2: *Simulation of a heterogeneous 2D object (blue is soft, red is stiff), coarsened to a single triangle. We pull from coarse node A using a spring, and nodes B and C are attached to their rest positions using springs too. From left to right: (i) fine mesh simulated with linear corotational elasticity; (ii) our corotational homogenization as described in Section 3.3, which closely resembles the previous case; (iii) coarse corotational formulation where materials are simply averaged, leading to evident error.*

on a fine submesh (with common rotation) can be written as:

$$[\mathbf{R}]\,\mathbf{K}\,[\mathbf{R}]^T\,\mathbf{x} = \mathbf{f} + [\mathbf{R}]\,\mathbf{K}\,\overline{\mathbf{x}}, \qquad (1)$$

where $\mathbf{x}$ and $\mathbf{f}$ are, respectively, nodal positions and forces, $\overline{\mathbf{x}}$ are rest positions, and $\mathbf{K}$ is the stiffness matrix.

To compute the stiffness matrix of each fine element, we simply adhere to basic principles [Sifakis and Barbic 2012] and integrate the tensor of material properties $\mathbf{E}$ over the volume of the element. Using quadrature points for the integration, the stiffness matrix of each element is $\mathbf{K}_e = \sum_i w_i\,\mathbf{B}_i^T\,\mathbf{E}_i\,\mathbf{B}_i$, where w_i is the quadrature weight, $\mathbf{B}_i$ is the matrix of derivatives of shape functions evaluated at the quadrature point, and $\mathbf{E}_i$ is the material tensor at the quadrature point, which can be formed from Young's modulus and Poisson's ratio. This formulation is interesting for the simulation of deformable medical images, as shown in some of our examples. In that case, each voxel of the medical image constitutes a quadrature point, and the quadrature weight is the voxel volume. In our implementation, based on tetrahedral elements and barycentric shape functions, the precomputation of per-element stiffness matrices simplifies to $\mathbf{K}_e = v\,\mathbf{B}_e^T(\sum_i \mathbf{E}_i)\mathbf{B}_e$, where v is the voxel volume and $\mathbf{B}_e$ is the matrix of derivatives of shape functions, which is constant on each element.

Let us break the mesh nodes into three sets to explicitly distinguish the various types of boundary conditions: coarse nodes (subindex c), fine nodes with Dirichlet boundary conditions (subindex d), and fine nodes with Neumann boundary conditions (subindex n). Dirichlet boundary conditions simply imply that nodal positions $\mathbf{x}_d$ are given. Neumann boundary conditions, on the other hand, imply that nodal forces are given. W.l.o.g., we consider linearized forces of the form $\mathbf{f}_n + \frac{\partial \mathbf{f}_n}{\partial \mathbf{x}_n}\mathbf{x}_n$, as in each Newton step of a problem with nonlinear forces. For coarse nodes, it is not necessary to specify the types of boundary conditions at this point, as they can be expressed on the coarse problem. Instead, we consider generic coarse forces $\mathbf{f}_c$.

With the distinction of the various sets of nodes, the linear corotational elasticity problem in (1) can be rewritten as:

$$[\mathbf{R}] \begin{pmatrix} \mathbf{K}_{cc} & \mathbf{K}_{cn} \\ \mathbf{K}_{nc} & \mathbf{K}_{nn} - [\mathbf{R}]^T \frac{\partial \mathbf{f}_n}{\partial \mathbf{x}_n}\,[\mathbf{R}] \end{pmatrix} [\mathbf{R}]^T \begin{pmatrix} \mathbf{x}_c \\ \mathbf{x}_n \end{pmatrix} = \qquad (2)$$

$$\begin{pmatrix} \mathbf{f}_c \\ \mathbf{f}_n \end{pmatrix} + [\mathbf{R}] \begin{pmatrix} \mathbf{K}_{cc} & \mathbf{K}_{cn} & \mathbf{K}_{cd} \\ \mathbf{K}_{nc} & \mathbf{K}_{nn} & \mathbf{K}_{nd} \end{pmatrix} \begin{pmatrix} \overline{\mathbf{x}_c} \\ \overline{\mathbf{x}_n} \\ \overline{\mathbf{x}_d} - [\mathbf{R}]^T \mathbf{x}_d \end{pmatrix}.$$

In the following, we derive the homogenization method for this corotational elasticity problem. We approach this derivation in three steps. First, we deal with the simplest problem, where all fine

nodes are unconstrained (i.e., all the boundary conditions are zero-force Neumann conditions). The homogenization for this simplest problem allows us to formulate a base coarse stiffness matrix and base nonlinear shape functions. Second, we add Dirichlet boundary conditions into the homogenization method. And third, we add Neumann boundary conditions.

3.3 Unconstrained Corotational Homogenization

Let us simplify problem (2) into a fine unconstrained elasticity problem, in the sense that no position constraints or forces are applied on fine nodes:

$$[\mathbf{R}] \begin{pmatrix} \mathbf{K}_{cc} & \mathbf{K}_{cn} \\ \mathbf{K}_{nc} & \mathbf{K}_{nn} \end{pmatrix} [\mathbf{R}]^T \begin{pmatrix} \mathbf{x}_c \\ \mathbf{x}_n \end{pmatrix} = \qquad (3)$$
$$\begin{pmatrix} \mathbf{f}_c \\ \mathbf{0} \end{pmatrix} + [\mathbf{R}] \begin{pmatrix} \mathbf{K}_{cc} & \mathbf{K}_{cn} \\ \mathbf{K}_{nc} & \mathbf{K}_{nn} \end{pmatrix} \begin{pmatrix} \overline{\mathbf{x}_c} \\ \overline{\mathbf{x}_n} \end{pmatrix}.$$

Applying *condensation* [Guyan 1965; Bro-Nielsen and Cotin 1996] to this problem, it is possible to compute the displacements of coarse nodes alone, by solving a linear problem of coarse size:

$$[\mathbf{R}] \, \mathbf{K}_h \, [\mathbf{R}]^T \, \mathbf{x}_c = \mathbf{f}_c + [\mathbf{R}] \, \mathbf{K}_h \, \overline{\mathbf{x}_c}, \qquad (4)$$

$$\text{with } \mathbf{K}_h = \mathbf{K}_{cc} - \mathbf{K}_{cn} \, \mathbf{K}_{nn}^{-1} \, \mathbf{K}_{nc}. \qquad (5)$$

$\mathbf{K}_h$ is the homogenized stiffness matrix of the coarse element, and nothing else but the Schur complement of the fine submatrix $\mathbf{K}_{nn}$.

Once coarse nodal positions are known, fine nodal positions can be computed as:

$$\mathbf{x}_n = [\mathbf{R}] \left(\overline{\mathbf{x}_n} + \mathbf{N} \left([\mathbf{R}]^T \, \mathbf{x}_c - \overline{\mathbf{x}_c} \right) \right), \qquad (6)$$

$$\text{with } \mathbf{N} = -\mathbf{K}_{nn}^{-1} \, \mathbf{K}_{nc} \text{ nonlinear shape functions.} \qquad (7)$$

The coarse homogenized corotational solution in (4) is identical to the one reached by Torres et al. [2014], who designed a coarsening method for a high-resolution *linear* elasticity problem, and applied the corotational formulation to the coarse problem. Then, thanks to our derivation, we can conclude that simply applying a corotational formulation to the homogenized linear problem is equivalent to deriving a homogenized problem from an unconstrained corotational problem with common rotation. As we show in the next section, our sound derivation of corotational homogenization has a practical impact when applied on problems with rich and interesting boundary conditions.

Fig. 2 demonstrates the application of unconstrained corotational homogenization on a simple 2D example. The first snapshot shows a fine corotational simulation. The second snapshot shows the behavior with corotational homogenization, which closely resembles the previous case. The third snapshot corresponds to a coarse corotational formulation where materials are simply averaged, leading to evident error.

4 Coarsening of Boundary Conditions

The previous section sets the basis for the derivation of our coarsening method, but limited to the unconstrained problem (3), not the full high-resolution problem (2) with arbitrary Dirichlet and Neumann boundary conditions. We start this section with a discussion of naïve methods for handling of boundary conditions, which fail due to limited accuracy, but also lack of robustness. Then, we propose a sound derivation of coarsening operations for the full high-resolution problem (2). The solution to arbitrary boundary conditions bears a computational cost that inevitably depends on the
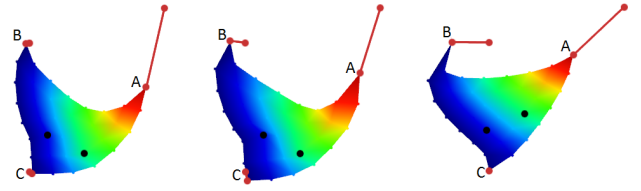
Figure 3: *Handling of fixed fine nodes (marked in black) under corotational coarsening. From left to right: (i) corotational fine mesh with fixed nodes, used for reference; (ii) our corotational homogenization with correct treatment of fixed fine nodes as described in Section 4.2, which closely resembles the previous case; (iii) homogenization with corotational formulation applied on the coarse setting, which fails to capture forces due to fixed fine nodes.*

complexity of the high-resolution mesh. However, we also design computationally efficient coarsening solutions for interesting types of boundary conditions, such as fixing arbitrary high-resolution points, the application of point forces at arbitrary locations, or volume contact constraints [Allard et al. 2010].

4.1 Naïve Handling of Boundary Conditions

We have demonstrated that, for the unconstrained problem, it suffices to coarsen a linear high-resolution problem and then apply the corotational formulation on the coarse setting. For handling of boundary conditions, it appears tempting to proceed similarly, designing a solution for the linear case, and extending this solution to the corotational formulation directly on the coarse setting. This turns out to be a bad idea, as we discuss next.
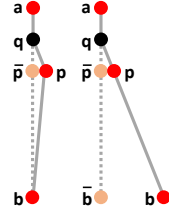
Handling of high-resolution Dirichlet conditions in the linear case is simple: fixed nodes are simply removed as degrees of freedom from the high-resolution problem. For the common case where nodes are fixed at their rest position, the homogenized problem (4) would simply be modified by recomputing the homogenized stiffness matrix $\mathbf{K}_h$ without the inclusion of fixed nodes. However, under a corotational formulation, nodes fixed at their rest positions produce non-zero forces, because they undergo a non-zero deformation $\mathbf{R}^T \overline{\mathbf{x}} - \overline{\mathbf{x}}$. The naïve coarsening solution produces the correct homogenized stiffness matrix, but it misses the coarse forces due to fixed high-resolution nodes, which do not even behave as being fixed! This effect is visible in the simple 2D example in Fig. 3, and also in our 3D comparisons.

Handling of high-resolution Neumann conditions appears as an exemplary candidate for the application of the *Jacobian transpose* method [Goldstein et al. 2001]: following the principle of virtual work, a force applied at an arbitrary position is transformed into a force on coarse nodes using the transpose of the Jacobian of this arbitrary position w.r.t. coarse node positions. The Jacobian transpose method is used profusely, e.g., for contact handling with high-resolution surfaces embedded in coarse deformable models. In the unconstrained coarsening solution (6), the Jacobian of high-resolution nodes w.r.t. coarse nodes is obtained simply by *warping* the shape functions $\mathbf{N}$ of the linear problem. Following the Jacobian transpose method in this case suffers two limitations that are not present in typical high-resolution surface embeddings. The first limitation is a lack of accuracy w.r.t. the high-resolution problem. The shape functions match accurately the motion of high-resolution nodes when they are unconstrained. However, they completely ignore the effect of high-resolution forces $\mathbf{f}_n$ shown in (2). In other words, the shape functions span only a limited subspace of deformations, those produced by forces applied on the coarse nodes,

while they ignore deformations produced by forces on fine nodes.

The second limitation is a possibly severe lack of robustness. In typical high-resolution surface embeddings, interpolation weights are positive and add up to one. Under our coarsening, instead, the shape functions $\mathbf{N}$ may not add up to one, due to extreme heterogeneity or fixed nodes. Then, stiff fine-node forces produce a lower net stiffness on coarse nodes, and even a small displacement of fine nodes may produce a large displacement on coarse nodes! The image on the side shows a notorious example, with a coarse 1D element with nodes $\mathbf{a}$ and $\mathbf{b}$. With a fixed high-resolution node $\mathbf{q}$ between $\mathbf{a}$ and $\mathbf{b}$, the shape functions for another high-resolution node $\mathbf{p}$ do not add up to one, e.g., $\mathbf{p} = 0 \cdot \mathbf{a} + 0.2 \cdot \mathbf{b}$. A small displacement $\mathbf{dp}$, handled well on the high-resolution deformation shown on the left, requires a much larger displacement $\mathbf{db} = 5 \cdot \mathbf{dp}$ using the Jacobian transpose method on the coarse element, as shown on the right. This effect is also visible in the simple 2D example in Fig. 4 and in our 3D comparisons.

In the rest of this section, we derive accurate and robust coarsening solutions for high-resolution boundary conditions.

4.2 Coarsening of Dirichlet Conditions

Following the condensation approach described in Section 3.3, we derive a coarsening method for Dirichlet conditions on a high-resolution corotational problem. Unfortunately, in the general case, accurate treatment of high-resolution Dirichlet conditions requires the solution of the fine elasticity problem at runtime. However, we have derived an efficient formulation of corotational homogenization for the common case where an arbitrary number of points are fixed at known positions (e.g., at their rest positions). We show that in this case, through application of a Fast Sandwich Transform (FST) [Kim and James 2011], both coarse and fine deformations produced by fixed fine points can be efficiently and accurately computed.

Let us rewrite the high-resolution corotational elasticity problem (2) considering Dirichlet boundary conditions, but limiting Neumann conditions to trivial zero forces:

$$[\mathbf{R}] \begin{pmatrix} \mathbf{K}_{cc} & \mathbf{K}_{cn} \\ \mathbf{K}_{nc} & \mathbf{K}_{nn} \end{pmatrix} [\mathbf{R}]^T \begin{pmatrix} \mathbf{x}_c \\ \mathbf{x}_n \end{pmatrix} = \quad (8)$$

$$\begin{pmatrix} \mathbf{f}_c \\ \mathbf{0} \end{pmatrix} + [\mathbf{R}] \begin{pmatrix} \mathbf{K}_{cc} & \mathbf{K}_{cn} & \mathbf{K}_{cd} \\ \mathbf{K}_{nc} & \mathbf{K}_{nn} & \mathbf{K}_{nd} \end{pmatrix} \begin{pmatrix} \overline{\mathbf{x}_c} \\ \overline{\mathbf{x}_n} \\ \overline{\mathbf{x}_d} - [\mathbf{R}]^T \mathbf{x}_d \end{pmatrix}.$$

Applying condensation to this problem, we obtain the following expressions for the computation of coarse and fine node deformations respectively:

$$[\mathbf{R}] \mathbf{K}_h [\mathbf{R}]^T \mathbf{x}_c = \mathbf{f}_c + [\mathbf{R}] \begin{pmatrix} \mathbf{K}_h & \mathbf{K}_{hd} \end{pmatrix} \begin{pmatrix} \overline{\mathbf{x}_c} \\ \overline{\mathbf{x}_d} - [\mathbf{R}]^T \mathbf{x}_d \end{pmatrix}, \quad (9)$$

$$\mathbf{x}_n = [\mathbf{R}] \left(\overline{\mathbf{x}_n} + \begin{pmatrix} \mathbf{N} & \mathbf{N}_d \end{pmatrix} \begin{pmatrix} [\mathbf{R}]^T \mathbf{x}_c - \overline{\mathbf{x}_c} \\ [\mathbf{R}]^T \mathbf{x}_d - \overline{\mathbf{x}_d} \end{pmatrix} \right), \quad (10)$$

with $\mathbf{K}_{hd} = \mathbf{K}_{cd} - \mathbf{K}_{cn} \mathbf{K}_{nn}^{-1} \mathbf{K}_{nd}$ the homogenized coupling stiffness of Dirichlet nodes, and $\mathbf{N}_d = -\mathbf{K}_{nn}^{-1} \mathbf{K}_{nd}$ nonlinear shape functions of Dirichlet nodes.

The original coarse equations (4) and (6) are augmented with force terms that depend on the Dirichlet conditions. If corotational elasticity is applied on the coarse setting after linear homogenization, these force terms are not present. The resulting errors can be seen in Fig. 3-iii.

In the general case, if the Dirichlet nodes are updated dynamically, position updates (9) and (10) require a full recomputation of homogenization, including the homogenized stiffness matrix $\mathbf{K}_h$. Let us now focus on the case where Dirichlet points are static. W.l.o.g., let us consider the case where fine points are fixed at their rest position, i.e., $\mathbf{x}_d = \overline{\mathbf{x}_d}$.

The coarsened Dirichlet forces in (9) and (10) require the computation of products of the form $\mathbf{A} \left([\mathbf{R}]^T \mathbf{x}_d - \overline{\mathbf{x}_d} \right)$, which for rest-position Dirichlet conditions turn into $\mathbf{A} \left[\mathbf{R^T} - \mathbf{I} \right] \overline{\mathbf{x}_d}$. With an average of N Dirichlet and Neumann nodes per coarse element, this product has a computational cost apparently as high as $O(N^2)$, due to the density of matrix $\mathbf{A}$. Recall, however, that $[\mathbf{R}]$ represents a large block-diagonal matrix with a common rotation matrix on each block. Then, for constant $\mathbf{A}$ and $\overline{\mathbf{x}_d}$, the coarse Dirichlet forces amount simply to linear transformations of the nine distinct elements of the rotation matrix $\mathbf{R}$. Therefore, the products can be rewritten as constant linear transformations of the nine-vector formed with the elements of $\mathbf{R}^T - \mathbf{I}$. Kim and James [2011] refer to this operation as the FST, and the products can be expressed as:

$$\mathbf{A} \, \overline{\mathbf{x}_d}^\star \left(\mathbf{R}^T - \mathbf{I} \right)^\star, \quad (11)$$

where $()^\star$ transforms a 3×3 matrix into the nine-vector with all its elements, and a $3n$ vector into the corresponding $3n \times 9$ matrix. The product $\mathbf{A} \, \overline{\mathbf{x}_d}^\star$ can be of course precomputed, and then the FST in (11) amounts at runtime to a weighted sum of the nine columns of $\mathbf{A} \, \overline{\mathbf{x}_d}^\star$.

Applying the FST, (9) and (10) can be efficiently solved as:

$$[\mathbf{R}] \mathbf{K}_h [\mathbf{R}]^T \mathbf{x}_c = \mathbf{f}_c + [\mathbf{R}] \begin{pmatrix} \mathbf{K}_h & \mathbf{K}_{hd} \overline{\mathbf{x}_d}^\star \end{pmatrix} \begin{pmatrix} \overline{\mathbf{x}_c} \\ (\mathbf{I} - \mathbf{R}^T)^\star \end{pmatrix}, \quad (12)$$

$$\mathbf{x}_n = [\mathbf{R}] \left(\overline{\mathbf{x}_n} + \begin{pmatrix} \mathbf{N} & \mathbf{N}_d \overline{\mathbf{x}_d}^\star \end{pmatrix} \begin{pmatrix} [\mathbf{R}]^T \mathbf{x}_c - \overline{\mathbf{x}_c} \\ (\mathbf{R}^T - \mathbf{I})^\star \end{pmatrix} \right). \quad (13)$$

The cost of coarse simulation according to (12) depends only on the resolution of the coarse mesh, and is on par with the cost of a regular coarse simulation. The update of fine nodes according to (13) reduces to a weighted combination of coarse node displacements and rotation terms, its cost is linear in the number of fine nodes, and can be massively parallelized.

Fig. 3 demonstrates how our corotational coarsening method succeeds in handling fixed fine nodes on a simple 2D example. The first snapshot shows a fine corotational mesh with fixed nodes. The second snapshot shows how our corotational homogenization closely matches the previous case. The third snapshot corresponds to a linear homogenization followed by corotational correction in the coarse setting, which fails to capture forces due to fixed fine nodes.

4.3 Coarsening of Neumann Conditions

Same as we did for Dirichlet boundary conditions, we follow the condensation approach described in Section 3.3 to derive a coarsening method for a high-resolution corotational problem including
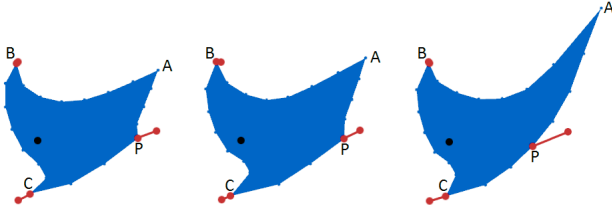
Figure 4: *Handling of fine node forces under corotational coarsening on a homogeneous object with a fixed fine node (marked in black). We pull from fine node P using a spring, coarse nodes B and C are attached to their rest positions using springs too, while coarse node A is left unattached. From left to right: (i) corotational fine simulation used for reference; (ii) our corotational homogenization with treatment of fine node forces as described in Section 4.3, showing accurate and stable deformation; (iii) corotational homogenization with treatment of fine node forces using the Jacobian transpose method, which leads to evident artifacts.*

Figure 5: *Contact handling as a ball collides with a heterogeneous triangle (blue is soft, red is stiff). Coarse nodes B and C are fixed with stiff springs, while A is left free. From left to right: (i) corotational fine simulation with a penalty-based collision per node, used for reference; (ii) our corotational homogenization, using a single volume contact constraint [Allard et al. 2010] as described in Section 4.3, showing almost identical behavior to the fine simulation; (iii) corotational homogenization with treatment of penalty-based collisions using the Jacobian transpose method, which leads to evident artifacts.*

both Dirichlet and Neumann conditions. Unfortunately, in the general case, accurate treatment of high-resolution Neumann conditions requires the solution of the fine elasticity problem at runtime. However, we have derived an efficient formulation of corotational homogenization for the interesting case where Neumann conditions stem from a few soft linear constraints (e.g., sparse springs or volume contacts). We show that in this case, Neumann conditions produce low-rank updates of high-resolution stiffness matrices, and both coarse and fine deformations can be efficiently and accurately computed through runtime modifications to the precomputed homogenized problem.
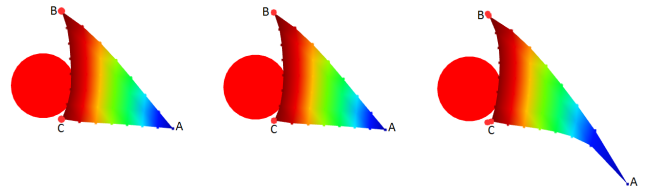
Let us revisit the full high-resolution corotational problem (2). For convenience, we define the stiffness term of Neumann nodes as $\widehat{\mathbf{K}_{nn}} = \mathbf{K}_{nn} - [\mathbf{R}]^T \frac{\partial \mathbf{f}_n}{\partial \mathbf{x}_n} [\mathbf{R}]$, and similarly modified Neumann forces as $\widehat{\mathbf{f}_n} = \mathbf{f}_n + \frac{\partial \mathbf{f}_n}{\partial \mathbf{x}_n} [\mathbf{R}] \, \overline{\mathbf{x}_n}$. The full high-resolution corotational problem (2) can be rewritten as:

$$[\mathbf{R}] \begin{pmatrix} \mathbf{K}_{cc} & \mathbf{K}_{cn} \\ \mathbf{K}_{nc} & \widehat{\mathbf{K}_{nn}} \end{pmatrix} [\mathbf{R}]^T \begin{pmatrix} \mathbf{x}_c \\ \mathbf{x}_n \end{pmatrix} = \tag{14}$$
$$\begin{pmatrix} \mathbf{f}_c \\ \widehat{\mathbf{f}_n} \end{pmatrix} + [\mathbf{R}] \begin{pmatrix} \mathbf{K}_{cc} & \mathbf{K}_{cn} & \mathbf{K}_{cd} \\ \mathbf{K}_{nc} & \widehat{\mathbf{K}_{nn}} & \mathbf{K}_{nd} \end{pmatrix} \begin{pmatrix} \overline{\mathbf{x}_c} \\ \overline{\mathbf{x}_n} \\ \overline{\mathbf{x}_d} - [\mathbf{R}]^T \mathbf{x}_d \end{pmatrix}.$$

In the remaining, we use the wide hat notation to denote all matrices that are modified dynamically due to the addition of Neumann forces, i.e., they are matrices whose computation needs to replace $\mathbf{K}_{nn}$ with $\widehat{\mathbf{K}_{nn}}$. Using this notation, and incorporating the FST from Section 4.2 into the treatment of static Dirichlet conditions, we apply condensation to the full high-resolution problem in (14), and we obtain the following expressions for the computation of coarse and fine node deformations respectively:

$$[\mathbf{R}] \, \widehat{\mathbf{K}_h} \, [\mathbf{R}]^T \mathbf{x}_c = \mathbf{f}_c + [\mathbf{R}] \, \widehat{\mathbf{N}}^T [\mathbf{R}]^T \, \widehat{\mathbf{f}_n} + \tag{15}$$
$$[\mathbf{R}] \begin{pmatrix} \widehat{\mathbf{K}_h} & \widehat{\mathbf{K}_{hd}} \, \overline{\mathbf{x}_d}^\star \end{pmatrix} \begin{pmatrix} \overline{\mathbf{x}_c} \\ (\mathbf{I} - \mathbf{R}^T)^\star \end{pmatrix},$$

$$\mathbf{x}_n = [\mathbf{R}] \left(\overline{\mathbf{x}_n} + \widehat{\mathbf{K}_{nn}}^{-1} [\mathbf{R}]^T \, \widehat{\mathbf{f}_n} \right) + \tag{16}$$
$$[\mathbf{R}] \begin{pmatrix} \widehat{\mathbf{N}} & \widehat{\mathbf{N}_d} \, \overline{\mathbf{x}_d}^\star \end{pmatrix} \begin{pmatrix} [\mathbf{R}]^T \mathbf{x}_c - \overline{\mathbf{x}_c} \\ (\mathbf{R}^T - \mathbf{I})^\star \end{pmatrix}.$$

These expressions take the same form as (12) and (13), augmented with terms due to fine Neumann forces $\widehat{\mathbf{f}_n}$, and with hatted matrices where appropriate.

Under arbitrary Neumann conditions, coarsening requires full recomputation of all hatted matrices. With an average of N Neumann nodes per coarse element and M elements in the coarse mesh, recomputing the homogenized stiffness matrices has a cost of solving roughly $12 M$ linear systems of size $3 N$, where 12 is the number of columns of $\mathbf{K}_{nc}$ in (5), i.e., the number of degrees of freedom of a tetrahedron. Let us now focus on the case where Neumann conditions stem from a few linear soft constraints.

Given a vector $\mathbf{c}$ of linear constraints, we define a soft-constraints energy $E = \frac{1}{2} \mathbf{c}^T \mathbf{W} \mathbf{c}$, with $\mathbf{W}$ a diagonal matrix of constraint weights (i.e., stiffness). We denote as $\mathbf{J} = \frac{\partial \mathbf{c}}{\partial \mathbf{x}_n}$ the constraint Jacobian. If the vector of constraints $\mathbf{c}$ is small, the force Jacobian $\frac{\partial \mathbf{f}_n}{\partial \mathbf{x}_n} = -\mathbf{J}^T \mathbf{W} \mathbf{J}$ is of low rank. As a result, the inverse of $\widehat{\mathbf{K}_{nn}}$ can be computed efficiently from the inverse of $\mathbf{K}_{nn}$ using the Sherman-Morrison-Woodbury (SMW) formula [Golub and Van Loan 1996; James and Pai 1999]:

$$\widehat{\mathbf{K}_{nn}}^{-1} = \mathbf{K}_{nn}^{-1} - \mathbf{K}_{nn}^{-1} [\mathbf{R}]^T \, \mathbf{J}^T \, \mathbf{K}_r \, \mathbf{J} \, [\mathbf{R}] \, \mathbf{K}_{nn}^{-1}, \tag{17}$$

with $\mathbf{K}_r = \left(\mathbf{W}^{-1} + \mathbf{J} \, [\mathbf{R}] \, \mathbf{K}_{nn}^{-1} \, [\mathbf{R}]^T \, \mathbf{J}^T \right)^{-1}$.

Substituting the SMW update of $\mathbf{K}_{nn}$ into the position updates (15) and (16), and after some arithmetic, we reach the following efficient expressions for all terms and products that involve hatted matrices:

$$\widehat{\mathbf{K}_h} = \mathbf{K}_h + \mathbf{N}^T \, [\mathbf{R}]^T \, \mathbf{J}^T \, \mathbf{K}_r \, \mathbf{J} \, [\mathbf{R}] \, \mathbf{N}, \tag{18}$$

$$\widehat{\mathbf{K}_{hd}} \, \overline{\mathbf{x}_d}^\star = \mathbf{K}_{hd} \, \overline{\mathbf{x}_d}^\star + \mathbf{N}^T \, [\mathbf{R}]^T \, \mathbf{J}^T \, \mathbf{K}_r \, \mathbf{J} \, [\mathbf{R}] \, \mathbf{N}_d \, \overline{\mathbf{x}_d}^\star, \tag{19}$$

$$\widehat{\mathbf{N}} = \mathbf{N} - \mathbf{K}_{nn}^{-1} \, [\mathbf{R}]^T \, \mathbf{J}^T \, \mathbf{K}_r \, \mathbf{J} \, [\mathbf{R}] \, \mathbf{N}, \tag{20}$$

$$\widehat{\mathbf{N}_d} \, \overline{\mathbf{x}_d}^\star = \mathbf{N}_d \, \overline{\mathbf{x}_d}^\star - \mathbf{K}_{nn}^{-1} \, [\mathbf{R}]^T \, \mathbf{J}^T \, \mathbf{K}_r \, \mathbf{J} \, [\mathbf{R}] \, \mathbf{N}_d \, \overline{\mathbf{x}_d}^\star, \tag{21}$$

$$\widehat{\mathbf{K}_{nn}}^{-1} \, [\mathbf{R}]^T \, \widehat{\mathbf{f}_n} = \tag{22}$$
$$\mathbf{K}_{nn}^{-1} \, [\mathbf{R}]^T \, \widehat{\mathbf{f}_n} - \mathbf{K}_{nn}^{-1} \, [\mathbf{R}]^T \, \mathbf{J}^T \, \mathbf{K}_r \, \mathbf{J} \, [\mathbf{R}] \, \mathbf{K}_{nn}^{-1} \, [\mathbf{R}]^T \, \widehat{\mathbf{f}_n}.$$

The computation of these terms involves solving $\mathbf{K}_{nn}^{-1} \, [\mathbf{R}]^T \, \widehat{\mathbf{f}_n}$ and $\mathbf{K}_{nn}^{-1} \, [\mathbf{R}]^T \, \mathbf{J}^T$, which total $1 + \text{sizeof}(\mathbf{c})$ linear-system solves with $\mathbf{K}_{nn}$. This matrix is constant; therefore, it is possible to precompute its Cholesky factorization or even its inverse (as we do in practice). The rest of the operations in (18)-(22) involve projections of

Figure 6: *Deformation of jelly stuffed with candy. The chocolates on the top are four orders of magnitude stiffer than the jelly, and the stiffness of 'Hard' and 'Soft' candy letters differs by six orders of magnitude. Our coarsening method retains this heterogeneity even with a regular 5K-tetrahedra mesh that is not aligned with object boundaries.*

the shape functions of Neumann nodes affected by the constraints into the constraint subspace. With a small number of constraints and with precomputed inverse $\mathbf{K}_{nn}^{-1}$, the operations in (18)-(22) bear up to an $O(N^2)$ computational cost per coarse element, but are massively parallelizable. Recall that N is the average number of Neumann nodes per coarse element.

We have tested two types of Neumann conditions in our examples: volume contacts [Allard et al. 2010] and sparse spring forces. With volume contacts, $\mathbf{J}$ tends to be sparse, and the cost of the position update (15) and (16) is $O(N)$ per coarse element. With sparse spring forces, $\mathbf{J}$ is a selection matrix, and the cost of the coarse position update (15) is $O(1)$, while the cost of the fine position update (16) is $O(N)$. Handling of Neumann conditions can be massively parallelized, as it is executed independently for each coarse element.

Fig. 4 demonstrates how our corotational coarsening method supports accurately and robustly a spring pulling from a fine node on a simple 2D example. We show the effect on a homogeneous model with fixed fine nodes. The first snapshot shows the reference result on a fine corotational simulation. The second snapshot shows the behavior with our corotational homogenization, demonstrating accurate and stable coarse deformation. The third snapshot corresponds to a corotational homogenization with treatment of fine node forces using the Jacobian transpose method, which leads to evident artifacts.

Fig. 5 demonstrates high-resolution contact handling with our method on a 2D heterogeneous triangle. The first snapshot shows the reference result on a fine corotational simulation with one penalty-based contact per colliding node. The second snapshot shows the behavior of our corotational homogenization using a single volume contact constraint for all colliding nodes. The behavior is almost identical to the fine simulation. The third snapshot corresponds to a corotational homogenization with treatment of penalty-based contacts using the Jacobian transpose method, which leads to evident artifacts.

5 Volume Resampling

For visualization, we wish to retain the geometric detail of the high-resolution discretization. For applications working with medical images, this translates into a deformation of a voxel grid. There are two major approaches to this problem: volume rendering with irregular meshes [Georgii and Westermann 2006] and volume resampling [Gascon et al. 2013]. We have opted for the second approach because it enables the use of the most advanced volume rendering techniques. Our algorithm is simple, yet very efficient on parallel architectures.

Before volume resampling, we interpolate on the GPU the coarse

deformation field to the full high-resolution mesh using (13). To do this, we upload coarse node positions and per-element rotation matrices to the GPU on every frame. Fine node positions and shape functions are stored only on GPU memory.

In our examples, we have used tetrahedra as high-resolution elements. Then, resampling of the voxel grid can be cast as a problem of tetrahedral rasterization with texture mapping. We execute this resampling fully on the GPU, as follows.

We start by computing the AABB of each tetrahedron in one thread, and then sort the tetrahedra by voxel-size of their AABBs, using the Thrust library in CUDA [Hoberock and Bell 2010]. Next, we arrange the sorted tetrahedra in groups, and we resize the AABB of all tetrahedra in the same group to the size of the largest AABB. For rasterization, we launch one GPU kernel per group, creating one thread per voxel of the AABBs of the tetrahedra in the group. With this strategy, it is trivial to identify tetrahedron-specific data based on the thread id. For our experiments, with tetrahedral meshes ranging from hundreds up to a million tetrahedra, we found that 100 groups offered a good trade-off between the variance in AABB size and the number of threads per kernel launch.

Each rasterization thread takes as input simply its thread id. It computes its 3D position using the vertex coordinates of the associated AABB, and then computes barycentric coordinates using the vertex coordinates of the associated tetrahedron. If the thread passes the barycentric inclusion test, it computes 3D texture coordinates through barycentric interpolation of per-vertex texture coordinates, and then executes a texture look-up from the original volume dataset using trilinear interpolation. The resulting value is written to the output voxel grid.

Our volume resampling algorithm is similar in spirit to the one by Gascón et al. [2013]. However, their algorithm generates target voxels by decomposing each tetrahedron into cells, and culling these cells on the CPU. As a result, the algorithm suffers a CPU cost that is linear in the number of high-resolution tetrahedra and scales badly in practice. In our algorithm, the CPU cost is limited to launching the required kernels. We generate more false-positive threads, but the overall strategy pays off, and we achieve over one-order-of-magnitude speed-up on our high-resolution examples. Resampling a 5-million-voxel grid with a 281K-tetrahedra mesh takes only 35.7 ms with our method, and over one second with theirs.

6 Experiments and Results

We have validated our coarsening method on three major examples of highly heterogeneous volumes: a jelly stuffed with candy (Fig. 6), a CT of a fish (Fig. 7), and a CT of a human abdomen (Fig. 1). All three examples were simulated using quasi-static deformation, on a 3.1 GHz Quad-core Intel Core i7-3770S CPU with
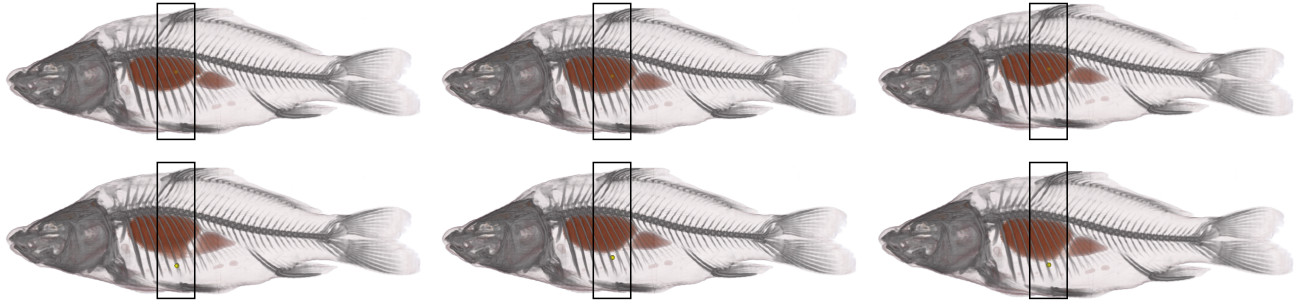
Figure 7: *Deformation of a fish CT, pulling up and down from its soft internal organs. The input CT scan is meshed with 135K heterogeneous tetrahedra, and we coarsen this model down to 5K tetrahedra. From left to right: (i) our method being pulled with a soft spring, (ii) a regular coarse simulation pulled with the same soft spring, and (iii) the regular coarse simulation pulled with a stiff spring. Our method correctly resolves materials at sub-element resolution, and the organs deform while the bones remain still. In the regular coarse simulation, on the other hand, materials get averaged out and the organs appear too stiff. With a soft spring, the organs do not deform; with a stiff spring, deformations are incorrectly transferred to the whole fish.*

16GB of memory, and a NVIDIA GTX670 graphics card.

Benchmarks Young's moduli of all the different materials present in the benchmarks are summarized in Table 1, and the resolutions of the tetrahedral meshes in Table 2. In all three benchmarks, our coarse simulation mesh is a regular mesh that is not aligned with the underlying geometry, yet the simulation preserves high-resolution heterogeneous behavior. Note also that the input material stiffness may differ by more than six orders of magnitude within the same benchmark.

To design the jelly benchmark in Fig. 6, we took as input the surface meshes of the jelly, the chocolates, and the 'Hard' and 'Soft' candy letters. With all the surface vertices as constraints, we created a high-resolution tetrahedral mesh using TetGen. We applied the Young's modulus of each input object to all the high-resolution tetrahedra contained in it.

For the fish CT data set in Fig. 7, we first assigned materials to opacity ranges through simple manual inspection of the complete opacity range. Then, we created a regular high-resolution tetrahedral mesh on top of the volume grid, and computed the material tensor of each high-resolution tetrahedron from per-voxel material properties following the procedure outlined in Section 3.2.

Finally, for the abdomen CT data set in Fig. 1, we slightly modified the meshing procedure used for the fish. We segmented bone material after visually identifying its opacity range, meshed the resulting bone surfaces, and created a high-resolution tetrahedral mesh by combining the bone nodes with a regular high-resolution grid in TetGen. In this benchmark, the high-resolution bone nodes are set as fixed, and are treated by our coarsening method as described in Section 4.2.

Comparisons and error evaluation In all three benchmarks, our method captures sub-element heterogeneity. Notice, for example, the deformation of the 'Soft' candy letters in contrast to the rigid motion of the 'Hard' letters in Fig. 6. With our method, the soft organs of the fish are discriminated from the stiff bones, as shown in the deformation examples in Fig. 7. With a regular coarse mesh, materials are averaged, and the organs appear stiffer than they should.
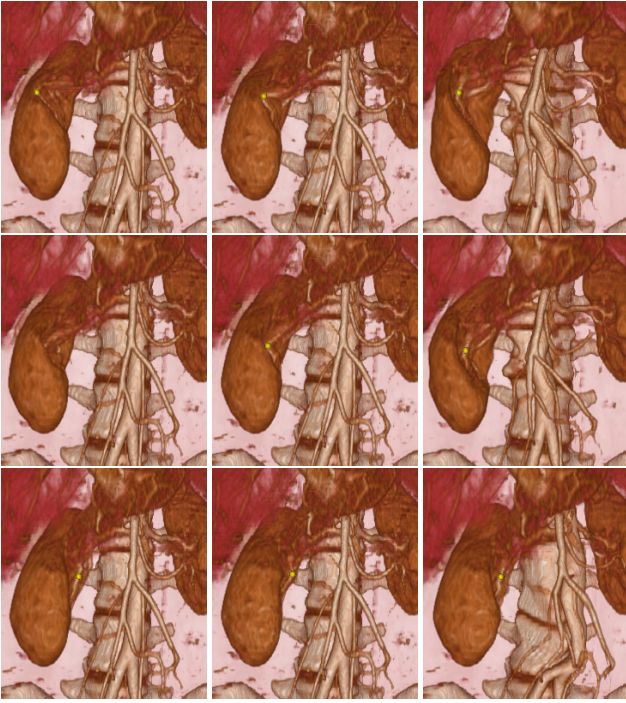
Thanks to robust and accurate handling of boundary conditions at arbitrary locations within the volume, we achieve attractive simulation features for medical imaging data sets in particular. Users may interact directly with the volume data set, select interaction points through ray casting of the visible isosurface, and perform interactive deformation of visible geometry. As shown in Fig. 1, our accurate handling of Neumann and Dirichlet conditions enables fine manipulation of thin features.

In Fig. 1 and Fig. 8, we also show contact interactions between a cylindrical tool and the abdomen CT data set. This setting is motivated by the applicability of our simulation method for preoperative planning of intraoperative electron-beam radiation therapy (IOERT) [Gunderson et al. 2011] on soft tissues. IOERT employs a cylindrical applicator introduced into the patient's body through the surgical opening, which deforms the tissues next to the region
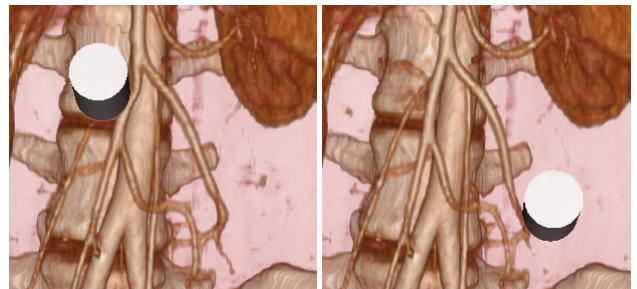
Figure 8: *Simulation of detailed contact between a cylindrical tool and fine vein geometry in the abdomen CT data set. We model high-resolution contacts using the volume contacts method [Allard et al. 2010], and then we coarsen them according to the general treatment of high-resolution Neumann boundary conditions described in Section 4.3. Please see the video for more evident contact deformations.*
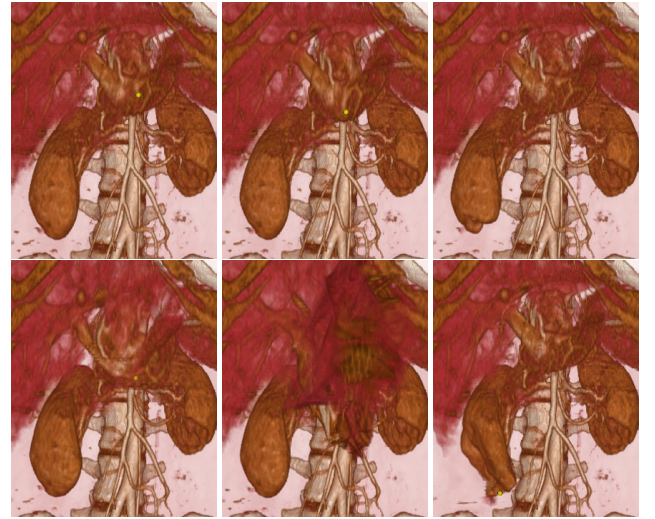
Jelly		Fish		Abdomen	
Jelly	1e3	Bones	5e8	Bones	fixed
Chocolates	1e7	Organs	1e3	Veins	1e5
'Hard'	1e8	Skin	4e5	Kidneys	1.9e4
'Soft'	1e2	Air	1e2	Liver	0.7e3
				Other	1.7e3

Table 1: *Young's modulus (in N/m^2) for the materials in the benchmarks.*

Figure 9: *Comparisons between a high-resolution simulation (left column), our method (middle column), and a low-resolution simulation (right column) on the abdomen CT data. In the low-res simulation, heterogeneity of the material is not well preserved and sub-element boundary conditions are not successfully enforced. Notice how the kidney does not admit local deformations, the backbone appears soft, and deformations from the kidney are transmitted to the veins. The deformations with our coarsening method, instead, match closely the deformations with the high-resolution simulation, at a cost comparable to the low-resolution simulation.*

Figure 10: *We compare the handling of Neumann boundary conditions on the abdomen CT data using our coarsening method (top) and using the Jacobian transpose method on the coarsening result of [Torres et al. 2014]. Under soft forces (left: pulling softly from the stomach), the Jacobian transpose method behaves reasonably well, although it already shows some noticeable error. Under strong forces (middle: pulling strongly from the stomach), however, it turns unstable. On some parts of the model, it produces unrealistic deformations even under moderate forces (right: pushing moderately on a kidney).*

to be radiated. For collision detection, we test for intersection with the cylinder all the visible fine nodes (according to the active transfer function of volume rendering). Then, we add high-resolution contact handling into the quasi-static simulation by coarsening the forces of the volume contacts model [Allard et al. 2010], as described in Section 4.3.

We have executed additional experiments and comparisons on the abdomen benchmark, as shown also in the accompanying video. Fig. 9 shows comparisons of a full high-resolution simulation, our method, and a regular coarse simulation. The artifacts of the coarse simulation are evident, in particular in the form of disconnected tissues that appear connected, or sub-element bone geometry that fails to remain fixed.

Fig. 10 depicts the handling of Neumann boundary conditions on the abdomen CT data. It compares our coarsening method against the application of the Jacobian transpose method on the coarsening result of [Torres et al. 2014]. The example clearly shows robustness and instability artifacts produced by the addition of forces on previous coarsening solutions using the Jacobian transpose method. Such naïve corotational coarsening works reasonably well in rather homogeneous and/or unconstrained areas; however, as discussed throughout the paper, the comparisons demonstrate that it fails in highly heterogeneous and/or constrained areas.

We have also quantified the accuracy of our coarsening method on the abdomen data set, in comparison to the full high-resolution sim-

ulation and a regular coarse simulation. In the coarse simulation, we use barycentric interpolation of coarse node positions to compute the positions of fine nodes. With our method, we use nonlinear interpolation as in (13) instead. We have executed 100 deformations of the abdomen data set, where each time we apply a 10-mm displacement at a random location using a stiff spring. For each deformation, we measure the maximum error w.r.t. the high-resolution simulation. In the regular coarse simulation, the average maximum error over all 100 deformations is 11.9 mm, and the total maximum error is 39.5 mm. With our method, the average maximum error over all 100 deformations is 1.6 mm, and the total maximum error is 3.1 mm. We achieve a dramatic reduction of average relative error from 119% down to 16%, and maximum relative error from 395% down to 31%.

Performance We have also evaluated the computational cost of our corotational coarsening method on the three benchmarks. Average deformation costs per frame are reported in Table 2, and our CPU solver runs at 30.4 fps (for the abdomen) to 14.4 fps (for the jelly, which requires more iterations of the linear solver on average). Performance is almost identical with a regular coarse simulation. In the simulation examples with contact handling, the overall impact of the potential $O(N^2)$ cost per coarse tetrahedron is negligible, because contacts are sparse and they affect only a small number of coarse tetrahedra.

With the full high-resolution simulation, we obtain frame rates that vary from 0.4 fps for the abdomen to approximately 0.2 fps for the jelly. Optimized FEM solvers, such as the one described in [McAdams et al. 2011], could notably improve the performance of the high-resolution simulation, but this is ultimately limited by mesh resolution. Table 2 also reports the computational cost for GPU-based nonlinear interpolation of coarse displacements to the fine nodes, which is just a fraction (roughly $1/5$) of the deformation

Benchmark	Fine (#tets)	Coarse (#tets)	Volume (#voxels)	Deform (ms)	Interpolate (ms)	Resample (ms)	Render (ms)
Jelly	320K	5K	-	69.4	12.1	-	-
Fish	135K	5K	20.5M	37.3	5.9	184.4	500
Abdomen	281K	6K	5M	32.9	6.9	35.7	25

Table 2: *Statistics and performance for the benchmarks: size of the original fine mesh and the coarse mesh; size of the volume grid; time per frame (in ms.) for elastic deformation with our coarsening method, interpolation of coarse deformations to the fine mesh, resampling of the volume grid, and volume rendering. The jelly benchmark is a ray-traced triangle mesh, hence some statistics do not apply.*

cost.

And finally, the last two columns indicate timings for GPU-based resampling of the volume grid and volume rendering (using VTK [Schroeder et al. 2004]), for the fish and abdomen benchmarks. For the abdomen, the full simulation and visualization, including deformation, interpolation, resampling, and high-resolution volume rendering of the deformed data set run interactively at 10 fps.

7 Discussion and Future Work

We have presented a method to simulate elastic deformations efficiently on coarse meshes, while respecting high-resolution heterogeneous behavior and boundary conditions. Our method is rooted on a principled derivation of numerical coarsening for linear corotational elasticity. This allows us to produce coarse simulation models that both accurately and robustly handle high-resolution boundary conditions. In addition, we achieve high computational efficiency on interesting types of boundary conditions, through careful application of linear algebra operations on the resulting equations.

Our method is approximate, hence it is also limited in nature. Compared to a full-resolution linear corotational model, we make several assumptions. First and foremost, we assume that local rotations are smooth and can be approximated at a low resolution; therefore, our method is not capable of reproducing high-resolution rotations. Second, while our model reduces the computational cost under general boundary conditions, it reaches maximum computational efficiency under static Dirichlet conditions and Neumann conditions that stem from a few soft linear constraints. Nevertheless, in our examples we demonstrate that this set of boundary conditions covers rich and interesting interaction modes.

Additional limitations are caused by the underlying model that we approximate, i.e., the stiffness warping framework for linear corotational elasticity. First, unlike the case of linear elasticity, the stiffness matrix is not an accurate Jacobian of elastic forces, and this could introduce instabilities in our solver, although we did not observe them except for extreme deformations. The accurate Jacobian would require the evaluation of derivatives of the rotation matrix, as derived by [Barbič 2012]. These accurate Jacobians could be added to our implementation in the coarse setting, and they do not affect the design of our homogenization method. Second, the elastic forces in stiffness warping are not conservative. A conservative corotational model can be obtained with the strain definition proposed by [Chao et al. 2010], but this would imply a different constitutive model and major changes to our homogenization approach. Third, our assumption of linear corotational elasticity prevents us from modeling other interesting behaviors such as hyperelasticity or high-resolution heterogeneous viscoelasticity. Finally, by extensively relying on precomputation, our method cannot support high-resolution topology changes.

We have demonstrated the success of our method for efficient yet accurate simulation of heterogeneous materials with high-resolution interactions. The method exhibits particularly high potential for medical image deformation in the context of relevant applications such as diagnosis, surgical planning, or intraoperative navigation.

Acknowledgements

References

ALLARD, J., FAURE, F., COURTECUISSE, H., FALIPOU, F., DURIEZ, C., AND KRY, P. G. 2010. Volume contact constraints at arbitrary resolution. *ACM Trans. Graph. 29*, 4, 82:1–82:10.

BARBIČ, J., AND JAMES, D. L. 2005. Real-time subspace integration for st. venant-kirchhoff deformable models. *ACM Trans. Graph. 24*, 3, 982–990.

BARBIČ, J., AND ZHAO, Y. 2011. Real-time large-deformation substructuring. *ACM Trans. Graph. 30*, 4, 91:1–91:8.

BARBIČ, J. 2012. Exact corotational linear FEM sitffness matrix. Tech. rep., University of Southern California.

BRO-NIELSEN, M., AND COTIN, S. 1996. Real-time volumetric deformable models for surgery simulation using finite elements and condensation. *Computer Graphics Forum 15*, 3, 57–66.

CAPELL, S., GREEN, S., CURLESS, B., DUCHAMP, T., AND POPOVIĆ, Z. 2002. A multiresolution framework for dynamic deformations. In *Proceedings of the 2002 ACM SIGGRAPH/Eurographics Symposium on Computer Animation*, 41–47.

CHAO, I., PINKALL, U., SANAN, P., AND SCHRÖDER, P. 2010. A simple geometric model for elastic deformations. *ACM Trans. Graph. 29*, 4, 38:1–38:6.

CHEN, D., LEVIN, D. I. W., SUEDA, S., AND MATUSIK, W. 2015. Data-driven finite elements for geometry and material design. *ACM Trans. Graph. 34*, 4, 74:1–74:10.

CIORANESCU, D., AND DONATO, P. 2000. *An Introduction to Homogenization*. Oxford University Press.

DEBUNNE, G., DESBRUN, M., CANI, M.-P., AND BARR, A. H. 2001. Dynamic real-time deformations using space & time adaptive sampling. In *Proceedings of the 28th Annual Conference on Computer Graphics and Interactive Techniques*, 31–36.

FAURE, F., GILLES, B., BOUSQUET, G., AND PAI, D. K. 2011. Sparse Meshless Models of Complex Deformable Solids. *ACM Transactions on Graphics 30*, 4, Article No. 73.

FILONOVA, V., LIU, Y., BAILAKANAVAR, M., FISH, J., AND YUAN, Z. 2013. Corotational formulation of reduced order homogenization. *Computers, Materials & Continua 34*, 3, 177–198.

GASCON, J., ESPADERO, J. M., PEREZ, A. G., TORRES, R., AND OTADUY, M. A. 2013. Fast deformation of volume data using tetrahedral mesh rasterization. In *Proc. of the ACM SIGGRAPH/Eurographics Symposium on Computer Animation*, 181–185.

GEORGII, J., AND WESTERMANN, R. 2006. A generic and scalable pipeline for gpu tetrahedral grid rendering. *Visualization and Computer Graphics, IEEE Transactions on 12*, 5, 1345–1352.

GOLDSTEIN, H., POOLE, C. P., AND SAFKO, J. L. 2001. *Classical Mechanics (3rd Edition)*, 3 ed. Addison-Wesley.

GOLUB, G. H., AND VAN LOAN, C. F. 1996. *Matrix Computations (3rd Ed.)*. Johns Hopkins University Press, Baltimore, MD, USA.

GRINSPUN, E., KRYSL, P., AND SCHRÖDER, P. 2002. Charms: A simple framework for adaptive simulation. *ACM Trans. Graph. 21*, 3, 281–290.

GUNDERSON, L. L., WILLETT, C. G., CALVO, F. A., AND HARRISON, L. B. 2011. *Intraoperative irradiation: techniques and results*. Springer Science & Business Media.

GUYAN, R. J. 1965. Reduction of stiffness and mass matrices. *AIAA journal 3*, 2, 380–380.

HARMON, D., AND ZORIN, D. 2013. Subspace integration with local deformations. *ACM Trans. Graph. 32*, 4, 107:1–107:10.

HOBEROCK, J., AND BELL, N., 2010. Thrust: A parallel template library. Version 1.7.0.

JAMES, D. L., AND PAI, D. K. 1999. Artdefo: Accurate real time deformable objects. In *Proceedings of the 26th Annual Conference on Computer Graphics and Interactive Techniques*, 65–72.

KHAREVYCH, L., MULLEN, P., OWHADI, H., AND DESBRUN, M. 2009. Numerical coarsening of inhomogeneous elastic materials. *ACM Trans. on Graphics 28*, 3, 51:1–51:8.

KIM, T., AND JAMES, D. L. 2011. Physics-based character skinning using multi-domain subspace deformations. In *Proceedings of the 2011 ACM SIGGRAPH/Eurographics Symposium on Computer Animation*, 63–72.

MALGAT, R., GILLES, B., LEVIN, D. I. W., NESME, M., AND FAURE, F. 2015. Multifarious hierarchies of mechanical models for artist assigned levels-of-detail. In *Proceedings of the 14th ACM SIGGRAPH / Eurographics Symposium on Computer Animation*, 27–36.

MCADAMS, A., ZHU, Y., SELLE, A., EMPEY, M., TAMSTORF, R., TERAN, J., AND SIFAKIS, E. 2011. Efficient elasticity for character skinning with contact and collisions. *ACM Trans. Graph. 30*, 4, 37:1–37:12.

MICHEL, J., MOULINEC, H., AND SUQUET, P. 1999. Effective properties of composite materials with periodic microstructure: a computational approach. *Computer Methods in Applied Mechanics and Engineering 172*, 14, 109 – 143.

MÜLLER, M., AND GROSS, M. 2004. Interactive virtual materials. *Proc. of Graphics Interface*.

NESME, M., KRY, P. G., JERÁBKOVÁ, L., AND FAURE, F. 2009. Preserving topology and elasticity for embedded deformable models. *ACM Trans. on Graphics 28*, 3, 52:1–52:9.

OWHADI, H., AND ZHANG, L. 2007. Metric-based upscaling. *Communications on Pure and Applied Mathematics 60*, 5, 675–723.

OWHADI, HOUMAN, ZHANG, LEI, AND BERLYAND, LEONID. 2014. Polyharmonic homogenization, rough polyharmonic splines and sparse super-localization. *ESAIM: M2AN 48*, 2, 517–552.

PANETTA, J., ZHOU, Q., MALOMO, L., PIETRONI, N., CIGNONI, P., AND ZORIN, D. 2015. Elastic textures for additive fabrication. *ACM Trans. Graph. 34*, 4, 135:1–135:12.

PENTLAND, A., AND WILLIAMS, J. 1989. Good vibrations: Modal dynamics for graphics and animation. *SIGGRAPH Comput. Graph. 23*, 3, 207–214.

SCHROEDER, W., MARTIN, K., AND LORENSEN, B. 2004. The Visualization Toolkit: An object-oriented approach to 3D graphics, 3rd edition. Tech. rep., Kitware Inc.

SCHUMACHER, C., BICKEL, B., RYS, J., MARSCHNER, S., DARAIO, C., AND GROSS, M. 2015. Microstructures to control elasticity in 3d printing. *ACM Trans. Graph. 34*, 4, 136:1–136:13.

SIFAKIS, E., AND BARBIC, J. 2012. Fem simulation of 3d deformable solids: A practitioner's guide to theory, discretization and model reduction. In *ACM SIGGRAPH 2012 Courses*, 20:1–20:50.

TENG, Y., OTADUY, M. A., AND KIM, T. 2014. Simulating articulated subspace self-contact. *ACM Trans. Graph. 33*, 4, 106:1–106:9.

TENG, Y., MEYER, M., DEROSE, T., AND KIM, T. 2015. Subspace condensation: Full space adaptivity for subspace deformations. *ACM Trans. Graph. 34*, 4, 76:1–76:9.

TORRES, R., ESPADERO, J. M., CALVO, F. A., AND OTADUY, M. A. 2014. Interactive deformation of heterogeneous volume data. In *Proc. of ISBMS*.